Integrated model calibration for anisotropy, hardening and rupture - Application to the clinching process

Abhishek Kumar, Ahmed Kacem, Sandrine Thuillier

Available online at www.sciencedirect.com

ScienceDirect

Procedia Structural Integrity 61 (2024) 62–70

Structural Integrity Procedia

www.elsevier.com/locate/procedia

3rd International Workshop on Plasticity, Damage and Fracture of Engineering Materials (IWPDF 2023)

Integrated model calibration for anisotropy, hardening and rupture - Application to the clinching process

Abhishek Kumar*, Ahmed Kacem and Sandrine Thuillier

Univ. Bretagne Sud, UMR CNRS 6027, IRDL, F-56100 Lorient, France

Abstract

To accurately predict the ductile rupture or failure using uncoupled rupture models for a given material, specific model parameters are required. These parameters are difficult to determine in a direct approach from experiments and need to be estimated using a hybrid experimental and numerical analysis, which accuracy relies on the quality of the anisotropy and hardening model calibration. In this study, material model parameters are estimated for AA6016-T4 and AA5182-O thin sheets. The methodology to determine material parameters of a combination of Swift-Voce hardening law and Yld2004-18p yield criterion is based on inverse identification over a full database made of quasi-homogeneous tests and specific rupture tests. The experimental data are obtained from sheet metal samples in the form of either stress-strain curves or load-displacement curves and local strain evolution measured by digital image correlation. To validate the simulation results, three additional tests on notched specimen are considered. The failure model parameters for a shear modified uncoupled Lou's rupture criterion are then determined using an average value of the triaxiality ratio and the Lode parameter at the material point of maximum equivalent plastic strain. The final aim of this study is the numerical prediction of the strength of a clinched joint of dissimilar AA6016-T4/AA5182-O sheets and the occurrence of rupture is numerically investigated at different stages.

Keywords: Material model calibration; Finite element analysis; Rupture tests; Sheet metal; Clinching

* Corresponding author. Tel.: +33 297 874 500
E-mail address: abhishek.kumar2@univ-ubs.fr

10.1016/j.prostr.2024.06.010

1. Introduction

The stringent environmental norms increase the use of advanced materials to manufacture lightweight vehicles. Often these advanced materials (aluminium alloy, polymer and composite) are difficult to join using conventional methods; in addition, dissimilar materials are used for reducing the weight. Clinching process gives an advantage over conventional joining process where sheet metals can be joint by plastic deformation at room temperature without any external material and heat source. It is an efficient and low-cost method of joining similar and dissimilar sheets. The clinched joint quality depends on the amount of undercut, neck thickness and bottom thickness of the sheet (Bielak et al., 2021).

Lambiase and Di Iilo (2013) used a 3D finite element model for clinching simulation with isotropic hardening (Ludwik law) to describe flow behaviour of the mild steel sheet. To predict the strength of clinched joints, a detailed finite element modelling approach was discussed by Coppieters et al. (2011). They developed 2D axisymmetric and 3D finite element model for clinching process using Abaqus/Explicit. The model predicts maximum force accurately during subsequent pull-out test, however underestimates the ductility. They reported that Voce hardening law-based model predicts a larger interlock of the joint. The accuracy of finite element predictions also depends on the material model parameters. Coppieters et al. (2011) used two different methods for post-necking hardening parameters identification, i.e., either multi-layered upsetting test with inverse identification method or digital image correlation (DIC) based tensile test experiments. Two different hardening law parameters were identified and both approaches showed an improved joint geometry prediction compared to the classical extrapolation method. Breda et al. (2017) used a mild steel sheet for evaluation of clinched joint strength and Swift hardening law was used for modelling the material behaviour. They calibrated the hardening law using force-displacement results of pull-out and shear lap tests. Identification of mechanical properties for clinching simulation could also be performed by bulge test, tensile test and layered compression test as discussed by Kupfer et al. (2022). These test methods represent different stress conditions which are important during clinching simulation.

Another important aspect of clinching simulation is damage or rupture prediction. Occurrence of failure during clinching was predicted by Lambiase and Di Ilio (2016) by incorporating Rice and Tracey criterion for an aluminium alloy. They calibrated the damage parameter using punch-out test, by matching the numerical results of force-displacement curve with experimental values. Coppieters et al. (2017) used finite element analysis to understand the bottom defect formation in clinched joint and its effect on the strength of a subsequent single lap shear specimen. For material behaviour, they used Swift and Voce-Xue laws and to predict the failure, Cockroft & Latham criterion, Rice & Tracey criterion, Modified Rousselier and the Inversely calibrated Modified Rousselier models were considered in the analysis. The parameters for hardening models were determined based on a methodology explained above (Coppieters et al., 2011) and damage parameters were determined by inverse method (Gou et al., 2013). Ma et al. (2022) studied the clinched bond formation during clinching of steel (JSC780) and aluminium (A5052-H34) alloy. They used Cockroft-Latham damage criterion to study the root cause of failure during clinching. In their study, a finite element model for clinching process was developed in Simufact Forming software. They predicted that a higher clamping force could result in neck cracking. Xu et al. (2021) studied the clinching process and strength of the clinched joint through numerical and experimental studies. They used Johnson-Cook hardening and damage model using Abaqus/Explicit software. They predicted the joint strength of Al7075 alloy and found that single lap joint strength was higher compared to the cross joint.

The framework of this study is the virtual clinching and subsequent mechanical testing of the clinched joints. As a first step, a hybrid experimental and numerical methodology was used to identify the material parameters for both AA6016-T4 and AA5182-O sheets. The parameters of an uncoupled shear modified Lou's rupture criterion are then estimated with the help of numerical analysis. Lou's rupture criterion is applied for failure prediction during clinching process. Further, clinched joint strength prediction is compared with experimental observations.

2. Methodology

2.1. Materials

The materials used in this study are AA6016-T4 and AA5182-O provided as 1 mm and 0.85 mm thick sheets, respectively. Basic mechanical properties of these materials are output from tensile tests and are given in Table 1. The aluminium alloy of 5000 series exhibits a higher stress level compared to the 6000 series one, a similar normal anisotropy coefficient but a rather insignificant planar anisotropy.

Table 1. Mechanical properties of the materials used for model calibration and clinching.

Material	Initial yield strength (MPa)	Tensile strength (MPa)	Young's modulus (GPa)	Normal anisotropy coefficient	Planar anisotropy coefficient
AA6016-T4	113.8 ± 1.29	229.0 ± 0.83	73.051	0.61	0.10
AA5182-O	152.0	293.0	72.073	0.68	0.03

2.2. Experiments

The mechanical behavior of the two materials was investigated at room temperature and under quasi-static conditions, with an average strain rate of the order of 10^{-3} s^{-1}, to characterize the anisotropy, hardening and occurrence of rupture. Tensile tests on dog bone specimen with a uniform central section, at 7 different orientations to the rolling directions, simple shear tests on rectangular specimen, in 3 orientations with respect to the rolling direction, hydraulic bulge test on circular blanks were performed. Repeatability was investigated over 3 to 5 samples and a representative test is chosen. Moreover, tensile tests on notched specimen, with different values for the notch radius, and specimen with a central hole and shear-type geometry were also performed for the rupture characterization in the rolling direction. Data given in Table 1 are calculated from these experimental results. Young's modulus values given in Table 1 are calculated as an average value of the initial slope of 5 loading-unloading cycles below the initial yield stress, using an extensometer. The strain field for all the other tests was captured using Digital Image Correlation (DIC) system ARAMIS. The geometries used are detailed in (Kacem et al., 2021, 2022). It must be emphasized that the full experimental database, including repeatability tests, amounts to a total of around 65 tests for each material.

2.3. Constitutive equations

The mechanical behavior is modeled within the large deformation framework, using isotropic hardening, described with a weighted Swift-Voce expression given by Eq. 1 coupled to the anisotropic yield criterion Yld2004-18p (Barlat et al. 2005), cf. Eq. 2.

$$\sigma_y(\bar{\varepsilon}_p) = \alpha\left[A(\varepsilon_0 + \bar{\varepsilon}_p)^{n}\right] + (1-\alpha)[\sigma_0 + Q\,(1-\exp(-b\bar{\varepsilon}_p))] \tag{1}$$

where $\bar{\varepsilon}_p$ is the equivalent plastic strain and α, A, ε_0, n, σ_0, Q and b are the parameters to be identified.

The Yld2004-18p criterion is given by Eqs. 2 to 4:

$$\emptyset = \sum_{i=1,j=1}^{3} \left|\bar{S}_i^{(1)} - \bar{S}_j^{(2)}\right|^{a} = 4\,\sigma_y^{a} \tag{2}$$

$$\tilde{S}^{(k)} = \tilde{L}^{(k)} : S\,, k = 1,2 \tag{3}$$

$$\tilde{L}^{(k)} = \begin{bmatrix} 0 & -c_{12}^{(k)} & -c_{13}^{(k)} & 0 & 0 & 0 \\ -c_{21}^{(k)} & 0 & -c_{23}^{(k)} & 0 & 0 & 0 \\ -c_{31}^{(k)} & -c_{32}^{(k)} & 0 & 0 & 0 & 0 \\ 0 & 0 & 0 & c_{44}^{(k)} & 0 & 0 \\ 0 & 0 & 0 & 0 & c_{55}^{(k)} & 0 \\ 0 & 0 & 0 & 0 & 0 & c_{66}^{(k)} \end{bmatrix}, k = 1, 2 \tag{4}$$

The parameter a in Eq. 2 is fixed and for FCC material its value can be considered as 8. The other 18 parameters of Eq. 3 were determined using hybrid numerical and experimental calibration process.

Lou's 2012 (Lou et al., 2012) rupture criterion can be given by Eq. 5. Here $D = 1$, represents the rupture and for this purpose C_1, C_2 and C_3 parameters were determined through experimental rupture tests and numerical analysis.

$$D(\bar{\varepsilon}_p) = \frac{1}{C_3} \int_0^{\bar{\varepsilon}_f} \left(\frac{2}{\sqrt{L^2+3}}\right)^{C_1} \left(\frac{\langle 1+3\eta \rangle}{2}\right)^{C_2} d\bar{\varepsilon}_p$$
$$\textit{Triaxiality ratio } (\eta) = \frac{\sigma_1+\sigma_2+\sigma_3}{3\bar{\sigma}}, \textit{ Lode parameter } (L) = \frac{2\sigma_2 - \sigma_1 - \sigma_3}{\sigma_1 - \sigma_3} \tag{5}$$

Here $\sigma_1 > \sigma_2 > \sigma_3$ represents the three principal stresses. For each material, there are 21 material parameters to describe hardening and anisotropy plus 3 more for the uncoupled rupture criterion. The model is implemented in a user subroutine for Abaqus/Standard. The calibration procedure is described in the following section.

2.4. Calibration procedure

The calibration for anisotropy and hardening is performed using all the tests, i.e., 7 tensile tests at different orientations to the rolling direction (including the stress level and the width strain), 3 simple shear tests also at different orientations to the rolling direction, a bulge test and 5 heterogeneous tests on notched specimen, specimen with a hole and tensile-like shear specimen. The first ones (tension, simple shear and hydraulic bulging) were considered quasi-homogeneous, and a finite element model made of only one cubic element, with boundary conditions leading to a homogeneous mechanical state is used for each type of test, to obtain numerical stress and strain data. However, a full finite element model is used for 3 rupture tests and the load, and the maximum local strain are output. The boundary conditions are output directly from the experimental measurements. The remaining 2 rupture tests are considered for a validation of the model.

$$S_{obj}(x) = \sum_{n=1}^{N} S_{obj}^{n}(x) \tag{6}$$

$$S_{obj}^{n}(x) = \frac{1}{n_p^n} \sum_{i=1}^{n_p^n} \left(\frac{Z_i^{exp}(t_i) - Z_i^{sim}(t_i, x)}{W_k} \right)^2 \tag{7}$$

where N is the number of tests and n_p^n the number of points for a given test, x the set of material parameters. Z_i^{exp} and Z_i^{sim} are the output variables coming from experiments and numerical simulation respectively. The weighting factor W_k ensures the standardization of unit from diverse output signal of the test, enabling comparability.

Inverse identification is carried out using SiDoLo software (Pradeau et al, 2016; Souto et al., 2015). The cost function, defined in the least square sense, quantifies the gap between the numerical predictions and the experimental values as given in Eq. 6 and 7. For each iteration, 14 finite element simulations are run, i.e., 11 with a single element

and the 3 others with a full model, for a given set of material parameters. The optimizer SiDolo determines a new set of parameters, and the cost function is then updated. When the gap is lower than a fixed value and/or the maximum number of iterations is reached, an optimized set of parameters is reached. The algorithm is based on Levenberg-Marquadt one and may be sensitive to local minima. Several sets of initial values were tried, to test the robustness of the presented values. This methodology ensures that a compromise is reached for the representation of all the tests in the database, both for hardening, anisotropy and rupture tests.

Finally, concerning Lou's model calibration, a classical hybrid experimental-numerical methodology is used. The maximum equivalent plastic strain, at a local displacement corresponding to the experimental value, is output. The average triaxiality ratio and Lode parameter at this material point are calculated and Lou's criterion parameters are then determined.

3. Results and discussion

3.1. Model calibration

In this section the inversely identified parameters are presented and the results are compared with experimental ones. In Fig. 1, the experimental and numerical comparison for some selected test results are shown. A good correlation for tensile loading in the rolling direction can be observed for both materials in Figs. 1 (a) and (d). Similarly, the results for shear tests, also performed in the rolling direction, are shown in Figs. 1 (b) and (e); however, bulge test results show a slight discrepancy both materials.

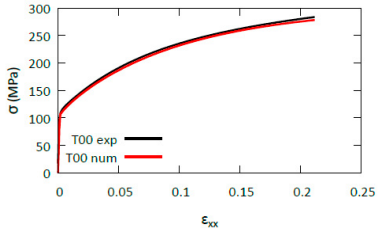

(a) AA6016-T4. Tensile test in RD

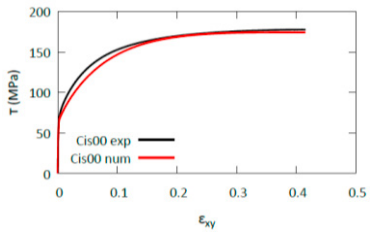

(b) AA6016-T4. Simple shear test in RD

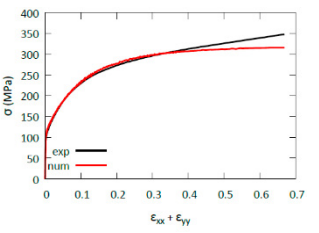

(c) AA6016-T4. Hydraulic bulge test

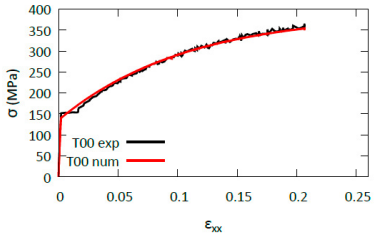

(d) AA5182-O. Tensile test in RD

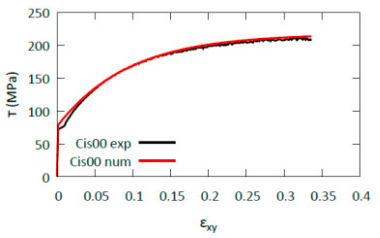

(e) AA5182-O. Simple shear test in RD

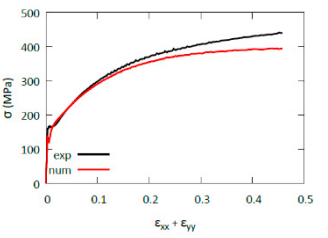

(f) AA5182-O. Hydraulic bulge test

Fig. 1: Experimental and numerical results comparison for different test conditions for model calibration (a-c) AA6016-T4 (d-f) AA5182-O.

Table 2: Yld2004-18p parameters calibrated from the experimental and numerical inverse identification procedure.

Material	$c_{12}^{(1)}$	$c_{13}^{(1)}$	$c_{21}^{(1)}$	$c_{23}^{(1)}$	$c_{31}^{(1)}$	$c_{32}^{(1)}$	$c_{66}^{(1)}$	$c_{12}^{(2)}$	$c_{13}^{(2)}$	$c_{21}^{(2)}$	$c_{23}^{(2)}$	$c_{31}^{(2)}$	$c_{32}^{(2)}$	$c_{66}^{(2)}$
AA6016	1.12	0.71	1.05	0.98	1.03	1.11	0.69	1.08	1.08	0.75	1.36	1.20	0.84	1.21
AA5182	1.11	0.95	0.92	1.22	1.12	0.78	1.08	0.86	0.86	0.92	0.90	1.02	1.09	0.85

Furthermore, the numerical predictions for the rupture tests were also compared with experimental observations for maximum strain values in critical region where the possible failure occurs, as shown in Fig. 2. Here it can be observed that the numerical results predict the maximum strain values and failure location with good accuracy under various

tests for both materials. The plastic anisotropy coefficients are very well predicted, as well as the stress levels, for all the orientations. These results confirm the effectiveness of the calibration methodology considered in the present study. The optimized set of parameter values are given in Tables 2 and 3.

Table 3: Swift-Voce parameters calibrated from the experimental and numerical inverse identification process.

Material	α	A (MPa)	ε_0	n	σ_0 (MPa)	Q (MPa)	b
AA6016	0.525	195.47	0.00335	0.118	123.76	355.21	11.219
AA5182	0.49	60.23	0.0059	0.0012	215.64	482.93	9.71

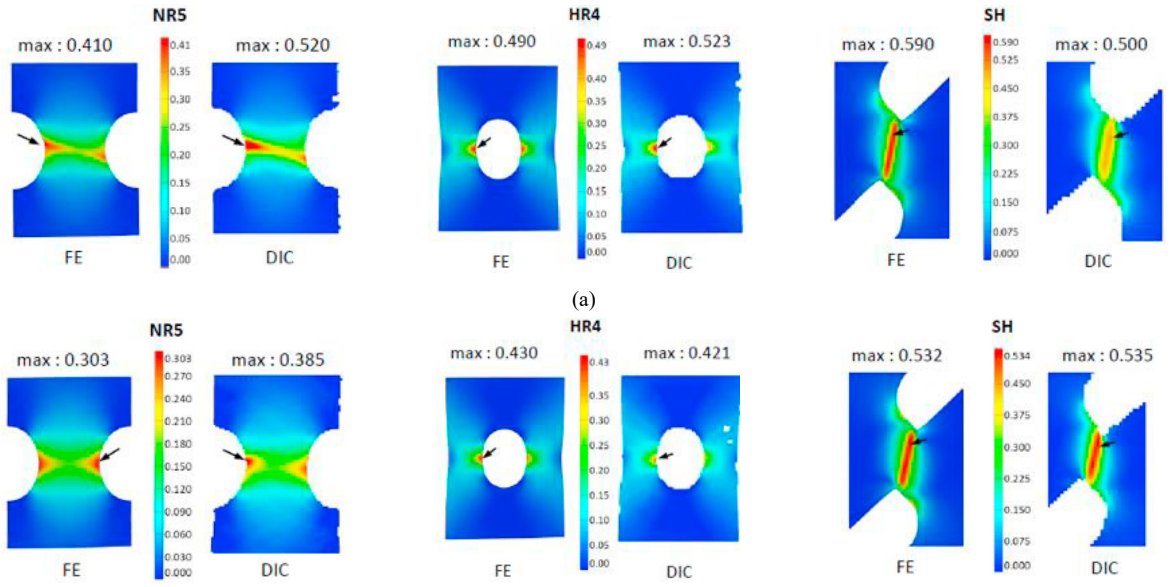

Fig. 2: Experimental (DIC) and numerical maximum strain comparison under various test conditions before rupture for (a) AA6016-T4 and (b) AA5182-O alloy.

Lou's rupture parameters were determined from the numerical results of the NR5, HR4 and SH geometries. Here, NR5 represents notch radius of 5 mm, HR4 hole diameter of 4 mm and SH is shear test sample. These parameters are given in Table 4 for both materials. The model calibration results can depend on the set of experiments considered (Yang et al., 2021) and the aluminium alloys may show weak effect on the Lode parameter as found previously by Qian et al. (2015). However, Zhang et al. (2020) found strong influence of Lode parameter for aluminium alloy and concluded the Lou's rupture criterion predicts fracture with good accuracy. In present study C_1 was found to be negative for both materials, as the limiting value of C_1 is 0 (Lou and Huh, 2013), therefore for failure analysis C_1 was considered as 0.

Table 4: Lou's 2012 rupture model parameters for identified from the numerical and experimental rupture analysis.

Material	C_1	C_2	C_3
AA6016-T4	0	0.562	0.605
AA5182-O	0	0.472	0.462

3.2. Clinching

The validation of the calibrated models was performed by the 3D finite element analysis of clinching process for AA6016-T4 and AA5182-O alloys and subsequent strength test of the clinched joint. In Fig. 3, clinching simulation

results can be observed, elements from the neck and bottom region (Fig. 3 (a)) are considered for the rupture and stress state analysis. In clinched joints, failure occurs mostly at the neck and bottom region of the sheet [8]. To understand the stress state in these regions, material points are selected from the top sheet for stress state analysis. Fig. 3 (a) shows the stress state for neck and bottom regions in stress triaxiality-Lode parameter plane. It can be observed that the stress state in the bottom region mostly remains as compression while in the neck region, points undergo near shear deformation (Jäckel et al., 2020). The stress state shows negative stress triaxiality for most of the considered points, only few material points show positive stress triaxiality, which might be due to a stretching of the sheet during clinching. To understand the possibility of failure during clinching, Lou's damage (D_{Lou}) values are calculated in the neck region for the upper sheet. Multiple material points are selected for the damage value calculation, however only 4 points could be used for the final analysis. This is due to the assumption of Lou's criterion that, at high negative stress triaxiality (< - 0.33), no failure occurs. The final damage value in the neck region w.r.t. equivalent plastic strain is shown in Fig. 3 (b). Here, failure in the material can be considered if the damage value reaches 1. The results in Fig. 3 (b) shows that the damage value remains below 1 in the neck region, hence no failure during clinching is predicted, which is in good agreement with experiments.

To further analyse the effectiveness of the present model, joint strength is predicted with a shear lap test. Fig. 4 (a) shows the different stages of the joint strength test, where instantaneous displacement of the bottom sheet is mentioned. These displacements are measured at the location corresponding to the displacement measured during experiments. This result shows the evolution joint condition where upper sheet detaches from one end of the joint and at the other end, strain localization occurs. The maximum strain value increases in the sheet neck region as observed in Fig. 4 (a).

(a) (b)

Fig. 3: Numerical results of clinching process (a) stress state after joint formation between AA5182-O and AA6016-T4 alloy (b) damage values after clinching process. PEEQ stands for the equivalent plastic strain.

A similar observation for similar aluminium alloy joint was noticed in a previous study (Köhler et al., 2021), however, the present study also shows similar failure evolution for dissimilar aluminium alloy joint. Another important factor for joint strength test is the maximum load capacity of the joint during shear loading. In Fig. 4 (b) a comparison of experimental and numerical joint strength can be observed. It can be seen that the present model predicts a lower maximum joint strength during the shear test. This might be due to neglecting the material anisotropy. However, the trend for the force evolution for the joint strength test was captured with good accuracy.

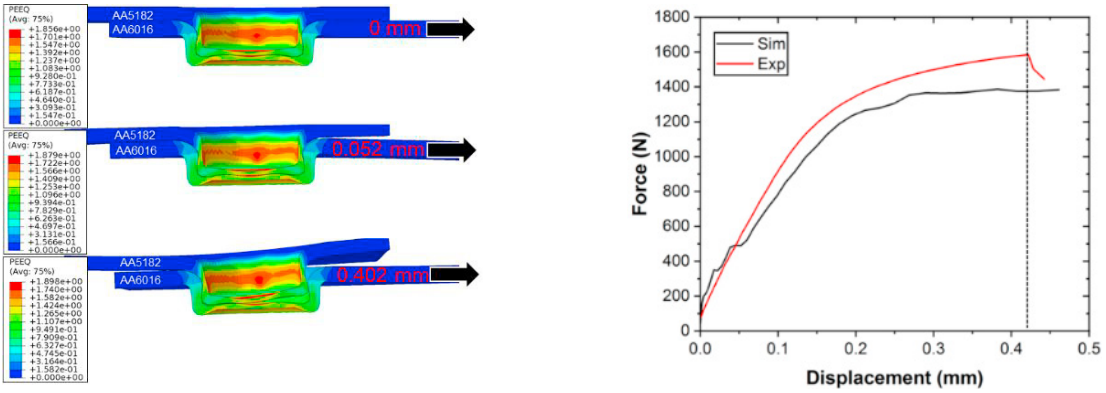

(a) (b)

Fig. 4: Numerical prediction of the rupture process during joint strength test for dissimilar joint of AA5182-O and AA6016-T4 alloy (a) evolution of the joint during shear test (b) force-displacement comparison of the clinch joint.

4. Conclusions

In this study, a hybrid methodology was used to calibrate the hardening, anisotropy and uncoupled rupture model parameters. The numerical and experimental observations show that the model was calibrated with good accuracy under different loading conditions to capture several stress states. These optimized material parameters were used for clinching simulation, which shows stress state evolution after clinch joint. Moreover, present model predicts no failure after clinching as observed during the experiment. Finally, the clinched joint strength for a shear-lap test is predicted and compared to the experimental.

References

Barlat F., Aretz, H., Yoon, J.W., Karabin M.E., Brem J.C., Dick R.E., 2005. Linear Transfomation-Based Anisotropic Yield Functions. International Journal of Plasticity, 21, 1009–39.

Bielak, Ch. R.., M. Böhnke, R. Beck, M. Bobbert, G. Meschut. 2021. Numerical Analysis of the Robustness of Clinching Process Considering the Pre-Forming of the Parts. Journal of Advanced Joining Processes, 3.

Breda A., Coppieters S., Debruyne D., 2017. Equivalent Modelling Strategy for a Clinched Joint Using a Simple Calibration Method. Thin-Walled Structures, 113, 1–12.

Coppieters, S., H. Zhang, F. Xu, N. Vandermeiren, A. Breda, D. Debruyne. 2017. Process-Induced Bottom Defects in Clinch Forming: Simulation and Effect on the Structural Integrity of Single Shear Lap Specimens. Materials and Design, 130, 336–48.

Coppieters, S., Cooreman S., Lava, P., Sol, H., Houtte, P.A., Debruyne, D., 2011. Reproducing the Experimental Pull-out and Shear Strength of Clinched Sheet Metal Connections Using FEA. International Journal of Material Forming, 4, 429–40.

Coppieters, S., Lava, P., Sol., H, Houtte P.A., Debruyne, D,. 2011. Identification of Post-Necking Hardening Behaviour of Sheet Metal: A Practical Application to Clinch Forming. Key Engineering Materials, 473, 251–58.

Guo, J., Zhao, S., Murakami, R.I., Zang, S., 2013. Experimental and Numerical Investigation for Ductile Fracture of Al-Alloy 5052 Using Modified Rousselier Model. Computational Materials Science, 71, 115–23.

Jäckel, M., Coppieters, S., Vandermeiren, N., Kraus, C., Drossel W.G., Miyake, N., Kuwabara, T., Unruh, K., Traphöner, H., Tekkaya, A.E., Balan, T., 2020. Process-Oriented Flow Curve Determination at Mechanical Joining. Procedia Manufacturing, Pp. 368–74.

Kacem, A., Laurent, H., Thuillier, S., 2021. Influence of Experimental Boundary Conditions on the Calibration of a Ductile Fracture Criterion. Engineering Fracture Mechanics, 248, 107686.

Kacem, A., Laurent, H., Thuillier, S., 2022. Experimental and Numerical Investigation of Ductile Fracture for AA6061-T6 Sheets at Room and Elevated Temperatures. International Journal of Mechanical Sciences, 222, 107201.

Köhler, D., Kupfer, R., Troschitz, J., Gude, M., 2021. In Situ Computed Tomography—Analysis of a Single-Lap Shear Test with Clinch Points. Materials, 14.

Kupfer, R., Köhler, D., Römisch, D., Wituschek, S., Ewenz, L., Kalich, J., Weiß, D., Sadeghian, B., Busch, M., Krüger, J., Neuser, M., Grydin, O., Böhnke, M., Bielak, C.R., Troschitz, J., 2022. Clinching of Aluminum Materials – Methods for the Continuous Characterization of Process, Microstructure and Properties. Journal of Advanced Joining Processes, 5.

Lambiase, F., Ilio, A.D., 2016. Damage Analysis in Mechanical Clinching: Experimental and Numerical Study. Journal of Materials Processing Technology, 230, 109–20.

Lambiase, F., Ilio, A.D., 2013. Finite Element Analysis of Material Flow in Mechanical Clinching with Extensible Dies. Journal of Materials Engineering and Performance, 22, 1629–36.

Lou, Y., Huh, H., Lim, S., Pack, K., 2012. New Ductile Fracture Criterion for Prediction of Fracture Forming Limit Diagrams of Sheet Metals. International Journal of Solids and Structures, 49, 3605–15.

Lou, Y., Huh, H., 2013. Extension of a shear-controlled ductile fracture model considering the stress triaxiality and the Lode parameter. International Journal of Solids and Structures, 50, 447-455.

Ma, Y., Abe, Y., Geng, P., Akita, R., Ma, N., Mori, K.I., 2022. Adhesive Dynamic Behavior in the Clinch-Bonding Process of Aluminum Alloy A5052-H34 and Advanced High-Strength Steel JSC780. Journal of Materials Processing Technology, 305.

Pradeau, A., Thuillier, S., Yoon, J. W., 2016. Prediction of Failure in Bending of an Aluminium Sheet Alloy. International Journal of Mechanical Sciences, 119, 23–35.

Qian, L. Y., Fang, G., Zeng, P., Wang, Q., 2015. Experimental and Numerical Investigations into the Ductile Fracture during the Forming of Flat-Rolled 5083-O Aluminum Alloy Sheet. Journal of Materials Processing Technology, 220, 264–75.

Souto, N., Campos, A.A., Thuillier, S., 2015. Material Parameter Identification within an Integrated Methodology Considering Anisotropy, Hardening and Rupture. Journal of Materials Processing Technology, 220, 157–72.

Xu, H., Zhang, Y., Peng, R., Zhu, L., Lu, Y., 2021. Simulation and Experimental Study on the Strength of Al7075-T6 Clinched Joint. Engineering Failure Analysis, 129.

Yang, Z., Zhao, C., Dong, G., Chen, Z., Sun, Y., Jia, X., 2021. Forming Limit Prediction of AA7075-T6 Sheet Based on Ductile Fracture Criterion and the Error Analysis of Parameters Calibration. International Journal of Material Forming, 14, 341–59.

Zhang, S., Lu, Y., Shen, Z., Zhou, C., Lou, Y., 2020. Prediction of ductile fracture for Al6016-T4 with a ductile fracture criterion: Experiment and simulation. International International Journal of Damage Mechanics, 29, 1199-1221.